EARTH SURFACE PROCESSES AND LANDFORMS
Earth Surf. Process. Landforms (2019)

Published online in Wiley Online Library
(wileyonlinelibrary.com) DOI: 10.1002/esp.4617

Sand particle velocities over a subaqueous dune slope using high-frequency image capturing

Renske C. Terwisscha van Scheltinga,[1]* Giovanni Coco[2] and Heide Friedrich[1]
[1] Department of Civil and Environmental Engineering, University of Auckland, Auckland, New Zealand
[2] School of Environment, University of Auckland, Auckland, New Zealand

Received 11 February 2018; Revised 13 March 2019; Accepted 25 March 2019

*Correspondence to: Renske C. Terwisscha van Scheltinga, Department of Civil and Environmental Engineering, University of Auckland, Auckland, New Zealand. E-mail: rgal477@aucklanduni.ac.nz

ESPL
Earth Surface Processes and Landforms

ABSTRACT: This work presents measurements and analysis of sand particle velocities over a subaqueous dune with median sand diameter of 0.85 mm. Time-lapse images of the mobile bed and an automated particle image velocimetry (PIV)-based cross-correlation method are used to obtain mean velocity of sand particles. This technique is shown to be consistent with measurements obtained with manual tracing. The measurements indicate an increase in mean particle velocity over a dune slope. Three regions are distinguished over the dune slope: (1) region of fluctuating particle velocity, (2) region of increasing particle velocity, and (3) region of maximum particle velocity. The observations are aligned with experimental and numerical modelling studies, indicating fluctuations in flow velocity over a dune stoss slope. We furthermore show that the standard deviation of the mean particle velocity is affected by the slope location and decreases from the lower slope towards the upper slope. The particle velocity variability is discussed in the context of general onset and cessation of sediment transport, the effect of the reattachment zone, sweep-transport events, and the existence of superimposed bedforms. With this work we bridge the gap between measurements of bedload transport at the particle-scale and at the bedform-scale. © 2019 John Wiley & Sons, Ltd.

KEYWORDS: sediment transport; particle motion; bedforms; PIV; laboratory experiments

Introduction

In experimental and field studies, measuring sediment transport without disrupting the flow and the sediment bed is challenging. Observations are that sediment particle transport occurs between phases of rest (repose time). Onset and cessation occur in four successive phases: entrainment, displacement, distrainment and repose (Drake *et al.*, 1988). Sand particles potentially move in different modes: rolling, sliding, saltating, and in suspension (Drake *et al.*, 1988; Nabi *et al.*, 2013; Yager and Schmeeckle, 2013). Rolling particles tend to move at small velocities. Saltating particles show long flights with a short phase of acceleration and a longer phase of decreasing velocity. Particle velocity and mode of transport are sensitive to changes in water depth, flow velocity, particle size and density, among others. Studies that trace particle motion for a large number (1000–10 000) of individual particles show that the distributions of the particle velocities can be fitted by an exponential law that monotonically decreases to zero for the streamwise direction. In the cross-stream direction, the velocities fit a Gaussian function (Drake *et al.*, 1988; Lajeunesse *et al.*, 2010; Roseberry *et al.*, 2012; Shim and Duan, 2017). Lajeunesse *et al.* (2010) show that particle motion is dominated by the mean value of the bed shear stress. Roseberry *et al.* (2012) focus on the degree to which particles are picked up randomly. They conclude that particle activity (the solid volume of particles in motion per unit area of streambed) and mean particle velocity increase log-linearly with increasing bed shear stress. Changes in the transport rate, with corresponding changes in stress, are dominated by changes in the activity, not the particle velocity (Roseberry *et al.*, 2012). Particle activity fluctuates as particles respond to near-bed fluid turbulence, whilst particles simultaneously interact with the bed. Roseberry *et al.* (2012) show that patchiness of particle movement occurs at the same timescale as that of turbulence sweeps. A larger sampling area will decrease the relative effect of the magnitude of the fluctuations compared to the overall level of activity. Furthermore, sediment particles show diffusive and advective behaviour, which is reflected in the fluxes directed from areas of high entrainment to low entrainment (Furbish *et al.*, 2017).

Particle movement is closely related to the development of bedforms. In the case of unidirectional currents, dunes are one of the most typical types of bedforms. Under unidirectional currents, dunes form under a selective range of flow conditions and sediment sizes (Southard and Boguchwal, 1990). Several studies aim to quantify dune migration and sediment transport flux over dunes (Van Rijn, 1984; Singh and Foufoula-Georgiou, 2013; Guala *et al.*, 2014; Venditti *et al.*, 2016). Dunes typically have a wedge shape, which causes flow to separate in the lee of the dune, and reattach 4–6 dune heights downstream of the crest (Best, 2005). The flow accelerates up the stoss slope, as a decrease in water depth causes flow conversion over the upward sloping bed of the dune stoss slope. Streamlines become compressed within the boundary layer over the rising stoss slope. As such, there is an interaction between the shape of the dune and the flow over the bed. To increase our

understanding of the complex interactions between the flow and the migrating dune, the quantification of the resulting sediment transport over the dune is a key element. Existing measurements of the sediment transport over dunes over a range of scales, from particle scale to bedform scale, are limited.

Progress in using imagery for sediment transport research is evolving, mainly due to advances in digital camera technology and in post-processing tools. The use of visualization techniques to measure sediment transport has proven to be reliable (Drake *et al.*, 1988; Lajeunesse *et al.*, 2010; Roseberry *et al.*, 2012; Yager and Schmeeckle, 2013; Fathel *et al.*, 2015; Shim and Duan, 2017). Using particle tracking velocimetry (PTV) and manual tracing, sediment transport studies are generally based on individual particle motion and are obtained at a limited range of conditions of flow velocity, water depth, and sediment size, predominantly for flat-bed conditions. These studies are not necessarily applicable to dunes, due to (i) variations in sediment sizes, (ii) non-uniform flow over the dune slope and (iii) higher mobility conditions. Visualization techniques to measure sediment transport, and not only individual particle motion, over dunes are limited (Tsubaki *et al.*, 2018). Figure 1 shows the existence of a measurement gap from high-frequency imagery for higher Shields numbers and lower Bonnefille numbers, which are conditions in which bedforms form. Exceptions are the measurements of Roseberry *et al.* (2012) and Nino and Garcia (1998). To avoid bedform formation, their measurements were obtained with a small slope (near hydraulic smooth conditions) or small water depth (< 0.05 m). The field of view in those studies was minimal (maximum of 1.5 × 1.3 cm and 7.6 × 1.1 cm), with a frame rate of 250 frames per second. Statistics are quantified based on individual particle motion over a fixed bed, and the authors acknowledged that their methods were time-consuming.

A procedure based on high-frequency imaging to measure sediment transport of natural sand over a mobile dune sediment bed is designed. The use of tracer particles is avoided by applying image subtraction and using subsequent images of difference (IoDs) to detect moving particles (Radice *et al.*, 2006; Shim and Duan, 2017). Manual particle motion tracing and a particle image velocimetry (PIV)-based cross-correlation technique (Ballio and Radice, 2007, Radice *et al.*, 2006) are combined to obtain a large number of mean particle velocities at different sections of the dune slope. The research questions underlying our work are: (1) How do measurements from a PIV-based cross-correlation technique compare to those from individual particle tracing, to obtain mean velocity of the moving particles? (2) How do sand particle velocities vary over a dune stoss slope? (3) What are the challenges towards quantifying mass flux of sediment over a dune using imagery? We demonstrate that PIV can be used to study bedload motion and we quantify spatial gradients in particle velocity over a dune bed. The method of cross-correlation on an IoD fills the gap between individual particle motion studies and measurements of average transport using sediment traps or bed morphology tracking.

Experimental Procedures and Analytical Methodology

Instrumentation

The experiments are conducted at the Water Engineering Laboratory at the University of Auckland (New Zealand). The flume is an 11.9 m long, 0.38 m deep and 0.44 m wide glass-sided open channel, with water and sediment recirculating capacity. Sediment dynamics are recorded with a high-speed camera recording at 90 frames per second, producing coloured images with a resolution of 2048 by 2048 pixels. The camera is placed 0.44 m above the initial sand bed level and the field of view covers the width of the flume. Camera and lens settings are used in manual mode, with specifications provided in Table I. Lens aperture is chosen to optimize sharpness, focus, exposure, chromatic aberration and sharpness towards the edges for the recorded images. Exposure is set as low as possible to mitigate noise (Mosbrucker *et al.*, 2017). Illumination is provided from the side of the flume and optimized to obtain equal illumination for the area of interest. A 1.1 m long acrylic sheet of 4 mm thickness is placed on the water surface to reduce refraction and the occurrence of water surface waves, as suggested by Heays *et al.* (2014) and Fathel *et al.* (2015). Without such a sheet, reflections from wavy water surface deteriorate image clarity and visibility of the sand grains. The dunes do not develop under 'covered' conditions, and the coverage area is of minimal length. Sediment transport studies under ice-covered surface have shown that the lower layer in a covered

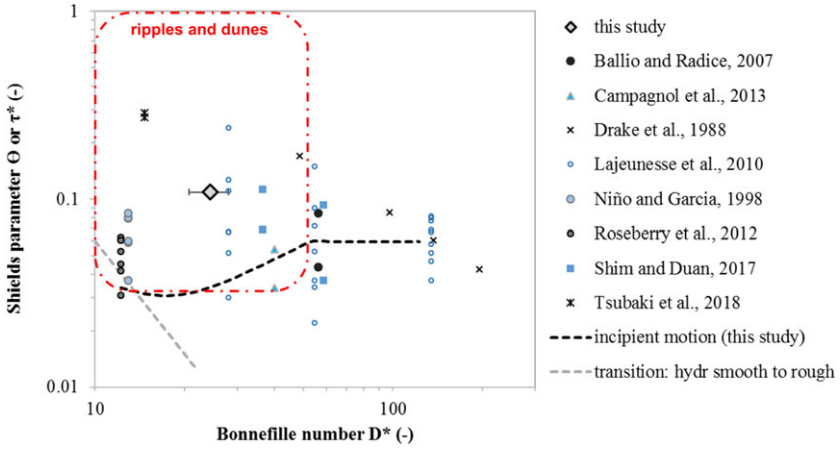

Figure 1. Experimental parameters for studies on sediment transport using high-frequency image capturing. Experiments performed under limited water depth conditions (< 0.06 m) have a label with a blue tint. Shield parameter (–) is a dimensionless measure for shear stress and is given by: $\theta = \frac{\tau}{(\rho_s - \rho)gD_{50}}$. With shear stress (in N/m^2) is: $\tau = \rho u^{*2} = \rho g h \sin S$, wherein ρ_s = sediment density (in kg/m^3), ρ = water density (in kg/m^3), g = acceleration due to gravity (9.81 m/s^2 on earth), D_{50} = median grain size (in metres), h = water depth (in metres) and S = water surface slope (–). Bonnefille number is a measure of sediment mobility and is given by $D^* = D_{50}\sqrt[3]{\frac{Rg}{\upsilon^2}}$, with $R = \frac{\rho_s - \rho}{\rho}$ being the relative submerged density, and υ the kinematic viscosity of water. Incipient motion is based on Vollmer and Kleinhans (2007) and the transition of hydraulic smooth to rough conditions on Kleinhans *et al.* (2017). [Colour figure can be viewed at wileyonlinelibrary.com]

Table I. Lighting, camera and lens settings

Lighting, camera and lens settings	
Illumination setup A	12 tubes of 1.5 m long (58 W; 4.800 lumen; cool daylight)
Camera	Lumenera LT425C
Lens	Samyang 10 mm/f2.8
Image resolution	2048 by 2048 pixels
Aperture	f/5.6
Lens height above initial sediment bed	0.44 m
Exposure setting	10 ms
Frame rate	1/90 s

flow can be treated as a free-surface flow for the purpose of calculating bedload transport (Lau and Krishnappan, 1985). Knack and Shen (2015) compared bedload transport measurements for covered conditions with bedforms and conclude that 'bed load transport can be described by conventional relationships for the equivalent free-surface flow if the flow strength is expressed in terms of the bed shear stress', p.1.

Experimental parameters

The flume is tilted at a slope of 0.0015 and filled with 0.1 m layer of uniform sand with a median grain diameter of 0.85 mm (Figure 2). Mean flow depth is 0.15 m and the mean flow velocity is 0.50 m/s. Flow velocities are measured with a Nortek Vectrino+ Acoustic Doppler Velocimeter and the flow at 40% of the water depth varies between 0.35 and 0.65 m/s. The depth-slope shear stress is 1.77 N/m^2. Near-bed velocities fluctuate due to acceleration and deceleration over dunes, in line with the turbulent nature of the flow and corresponding flow separation deattachment and reattachment (Best, 2005). The complex flow environment is reflected in a wide spread of shear velocity. Yager *et al*. (2018) provide a detailed discussion on the dissimilarity between different methods of measurements of shear stress and shear velocity. In our case, shear velocity obtained from flow profile measurements over a fixed plane bed is u^* = 0.021 m/s, whereas the shear velocity derived from the average depth-slope is u^* = 0.01 m/s. Other studies have provided general flow parameters for small water depths and a range of flow velocities over dune beds, which we assume to be valid for our experiments, and thus refer to (Maddux *et al*., 2003; Venditti, 2007; Nabi *et al*., 2012; Lockwood *et al*., 2018). Data recording was performed over nine dunes, with flow conditions kept constant for more than four hours after the dunes were in equilibrium condition. Calculations of mass flux of sediment are usually done in two separated modes, namely, bedload transport and suspended load transport (Van Rijn, 1987). The transport stage determines which mode is dominant (Venditti *et al*., 2016), with our experiments being in the bedload dominated stage. Dune migration rate approached 0.035 m/min.

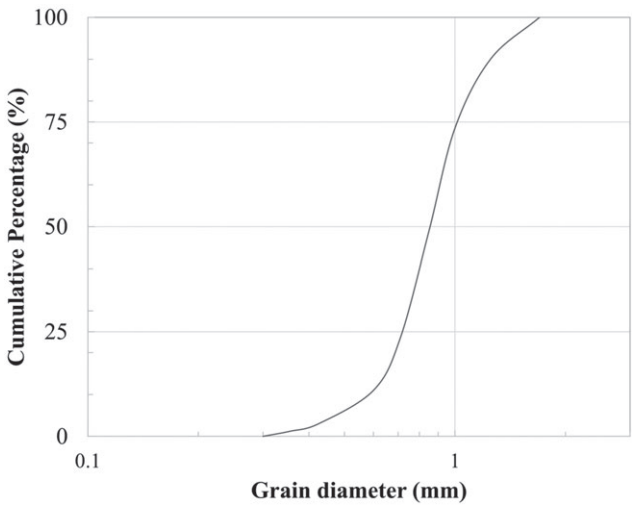

Figure 2. Grain size distribution of the natural sand.

Data collection and image processing (spatial and temporal analysis)

Images are recorded at high-frequency and cover an analysis area of 0.44 m width and 0.44–0.46 m streamwise length (depending on bed surface height, due to migrating dunes), as in Figures 3A–3C. To transfer particle velocity in pixels per frame to metres per second, the length scale of a pixel is needed, and the time step between two frames. For a fixed plain bed, the pixel length scale is fixed. However, our observations are collected for a changing sediment bed and the bedforms exhibit a well-defined slope. This implies that the pixel length scale varies within an image and between images, as a function of bed height. The pixel length scale in the vertical direction of an image is calculated by dividing flume width (0.44 m) with the total count of pixels covering the sediment bed in the vertical direction (Figure 3C).

Images are processed from dng-format into tif-format using dcraw.exe in Matlab R2016b (Coffin, 2009). Existing codes by Sumner (2014) and Luijk (2007) have been edited to account for our configuration. Camera and lens calibration are performed using the camera calibration toolbox application provided in Matlab R2016b and verified using the camera calibration toolbox for Matlab®, developed by J. Y Bouguet and available on the internet (Bouguet, 2010). An important image processing step to trace particle displacement is the step of segmentation (detection) of moving particles (Tal *et al*., 2012). Our method for detecting moving particles involves subtracting subsequent colour images of the natural sediment of the mobile bed (Radice *et al*., 2006, Shim and Duan, 2017). After image subtraction, conversion to greyscale and noise removal are applied to obtain an IoD between two time steps. The IoD exhibits a contrast in black and white (greyscale) between the locations in the image where a particle changed position and locations in the image where no particle changed position (monocolour background).

Plan-view images are recorded over the dune (Figure 4). The first image series covers 10 seconds over the trough and the upstream crest. The second image series is recorded three minutes later, with the location of the camera kept constant. Subsequently, seven image series are recorded with three and four minutes in between each series. Figure 4 shows that every cross-section in an image series is assigned a dune section reference length between zero and one. The dune's lee slope is relatively steep, since avalanching processes occur down the lee slope. The dune crest is two-dimensional in shape. Analysis of the sediment transport is done in the centre of the flume, covering 0.16 m flume width. The area near the flume wall is not considered, because the wall is likely to affect sediment transport. Results from recordings over the trough regions are not presented. Transport of particles is observed to occur up to several centimetres above the bed in the trough region. Images are recorded at 90 frames per second and IoDs are obtained for

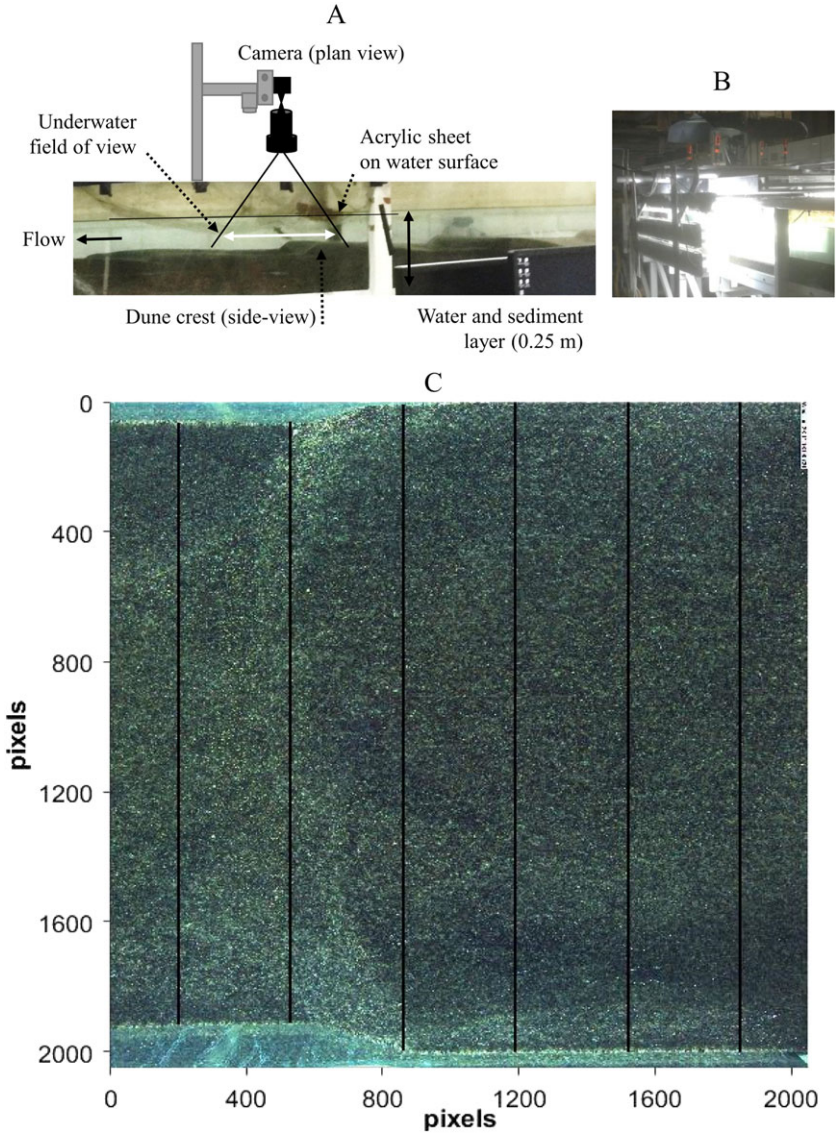

Figure 3. Experimental set-up, with the high speed camera on a fixed frame looking downwards; acrylic sheet on the water surface; flow from right to left; mobile sediment bed with dune morphology (A). Illumination is from the side (B). Example from image series 2, showing plan view over the dune crest and upper slope (C). The number of pixels at the vertical lines that cover the sediment bed changes as a function of sediment bed height. The bed level is higher, when less of the flume wall is visible. Image resolution is 2048 by 2048 pixels. [Colour figure can be viewed at wileyonlinelibrary.com]

images recorded at 2/90 second (hereafter 0.022 seconds) apart. If a lower threshold is chosen, for example 1/90 second, particles that travel slower than 0.075 m/s move less than median particle size, which is not suited for our analysis. As a result, the slowest travelling particles are not captured in the IoD. While, for a higher threshold, such as 3/90 or 4/90 second, identification of individual particle trajectories and of variability in particle displacement is difficult. The time step 0.022 seconds is a compromise between capturing slow moving particles and retrieving information on variability in particle behaviour.

Automated analytical methodology

Complementary to manual tracing of particle displacement, we used an automated PIV-based cross-correlation method to obtain the mean velocity of moving particles in a predefined area. PIV is commonly used to analyse the flow field. Radice *et al*. (2006) successfully applied PIV to track bedload motion. PIVlab is an open-source tool for analysis of digital particle image velocimetry (DPIV) developed by Thielicke and Stamhuis (2014). The DPIV-technique calculates particle displacement for particle groups. Cross-correlations between particle groups in two subsequent images are evaluated and provide the most probable displacement of the particles in a subpart of the image, assuming the particles travel in a straight line from image A to image B (Raffel *et al*., 2007). The analysis is sensitive to the choice of the size of the interrogation area (IA), among other pre-processing factors (Lewis and Rhoads, 2015). A different size of IA yields different velocity data time series for the same extraction location. Lewis and Rhoads (2015) show that a small IA and short time steps provide more details on particle displacement, but does not necessarily provide more accurate results. The size of IA and time step needs to be chosen carefully as a function of particle displacement variation (magnitude and orientation), while also considering the number and size of particles in an IA. In the study by Ballio and Radice (2007), PIV on IoD was used for bedload motion and validation was provided. A good correspondence is found for the average values for the sediment rate, when counted manually compared with image processing. Sediment

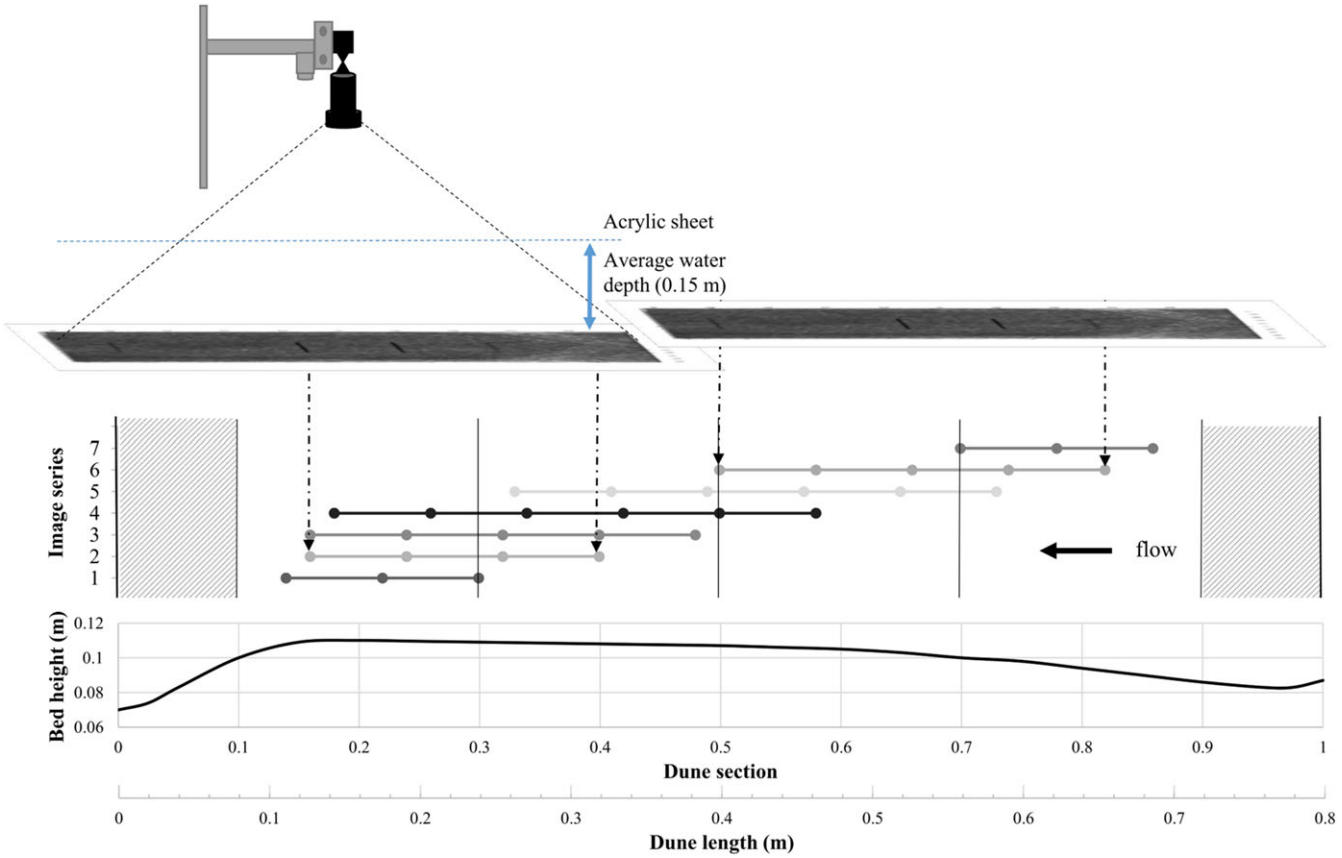

Figure 4. Seven series of images are recorded over a dune slope at a frame rate of 90 frames per second. Dots indicate the locations of the cross-sections and every cross-section is assigned a dune section value between zero and one. Zero represents the bottom of the dune lee slope and one represents the bottom of the streamwise dune lee slope (trough). The area of analysis is between 0.1 and 0.9. [Colour figure can be viewed at wileyonlinelibrary.com]

transport rates varying within two orders of magnitude are correctly measured (except for very low solid discharges). Their study was for weak transport of 3 mm (light-weight) grains. The work of Tsubaki *et al.* (2018) is more similar to the conditions of the present study (sand motion over dunes). An ensemble correlation PIV approach is used to cope with the 'limited image quality', which is valid for image sets recorded at high spatial and temporal resolution relative to the scale of turbulence, according to Westerweel *et al.* (2004).

To evaluate the measurements of mean particle velocity from cross-correlation on IoDs, we created a validation dataset using manual tracing. The location was on the upper part of the dune stoss slope. We manually traced ~40% of the particles identified in the IoD as moving particles (Figure 5). A sensitivity study is performed for different choices of IA. It is found that mean particle displacement approaches a constant value if the smallest IA is higher than 80 pixels (~ 0.018 m). When an IA of smaller than 30 pixels (~ 0.007 m) is chosen, the outcome is unreliable due to an insufficient number of particles moving within the IA. Regression analysis shows that for a small IA, cross-correlation analysis results in higher displacement compared to our manual displacement tracing. For an increasing IA size, the obtained vectors from the cross-correlation analysis results in lower displacement compared to manual tracing. Best agreement between the two procedures is obtained for an IA between 40 and 60 pixels. The density of tracked particles is not equally distributed over the area. On average, 5.2 particles are traced within an IA of 60 by 60 pixels (0.013 by 0.013 m) as in Figure 6. Thereafter, an averaging procedure was performed, in which one velocity vector was calculated from four neighbouring IAs and results are presented in Figure 7, showing agreement between the two methods. Results on pixel displacement of the two procedures are within the same range. The manual tracing validation set was used to find the 'optimum' settings for the automated PIV calculations for our images. To further enhance the quality of the spatial-average estimator, we apply ensemble averaging of the spatial correlation estimate to 10 successive image pairs as described in Westerweel *et al.* (2004) and Tsubaki *et al.* (2018). This procedure gives reliable results for situations of Brownian motion and low image density using micro-PIV (small tracer particles observed at high magnification).

Results

Particle velocity: double averaging procedure

Figure 8 shows particle trajectories for 16 moving particles traced in an area of 0.026 by 0.026 m and visualized for 10 time steps. The colour intensity represents the time step. Figure 8 illustrates (i) a variability of particle displacement between time steps and between particles in the area; (ii) the onset or cessation of particle motion or both within the time of analysis of 10 time steps (0.22 seconds); and (iii) that particles travel in different cross-stream directions. Figure 9 presents the streamwise velocity (u) of the particles trajectories in Figure 8. Rather than exhibiting a constant value, particle velocity varies due to the process of onset and cessation of moving particles. A short analysis period, for example 0.022 seconds, yields variable results for the instantaneous velocity (black dots). By averaging over a time period, we obtain a time-averaged particle velocity (grey dots in Figure 9A). A spatially averaged velocity varying in time (Figure 9B) is obtained by averaging the particle velocities in the

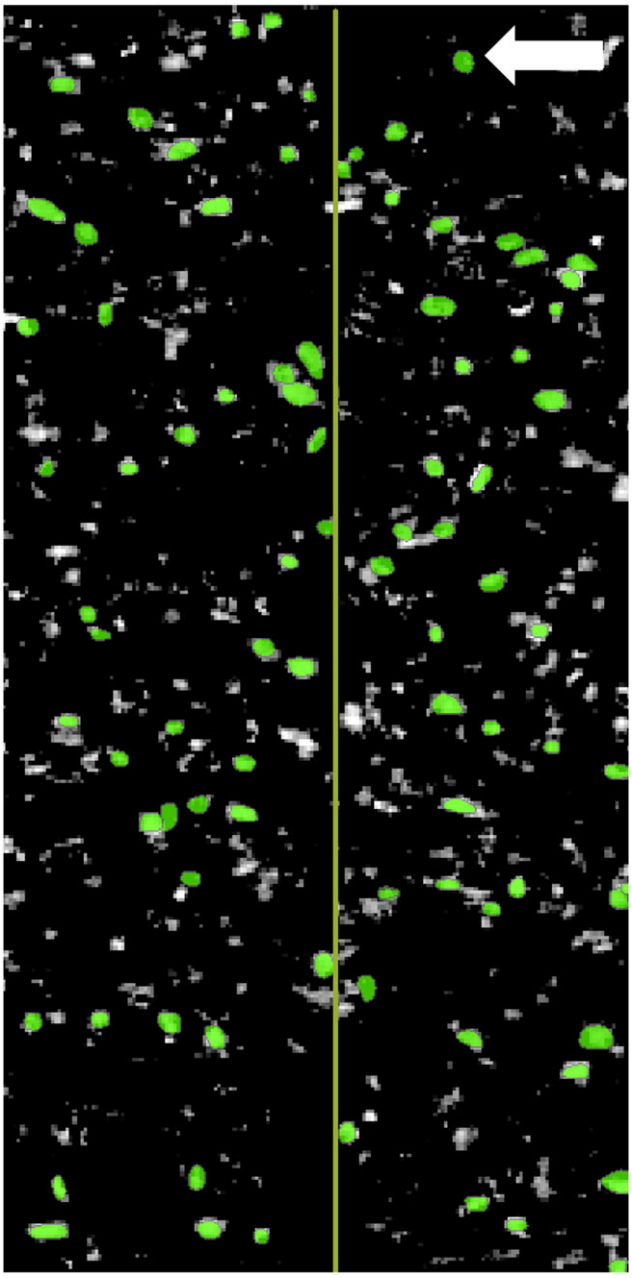

Figure 5. Display of image of difference (IoD) with manually traced particles (green). White are the moving particles and black is no movement. Window size is 340 by 140 pixels (0.075 by 0.03 m) and the line represents the cross-section location. [Colour figure can be viewed at wileyonlinelibrary.com]

area. The double-averaging procedure implies both spatial and time averaging, resulting in mean streamwise particle velocity (u), mean cross-stream particle velocity (v) and mean particle velocity (w).

The mean streamwise particle velocity in the area is 0.055 m/s for an analysis period of 0.22 seconds. The high variability in particle velocity of the individual particles is reflected in the standard deviation being large (0.038 m/s), compared to the mean of the 16 particles. For an analysis time of 0.22 seconds, not a single one of the particles has a mean velocity that resembles the overall mean, and approximately half of the particles move faster and half move slower than the mean of all the particles. Six out of 16 particles have a mean streamwise velocity that falls within one standard deviation, while mean velocities of all particles fall within two standard deviations from the overall mean. The spatially averaged particle velocity of the group of 16 particles varies less than the time-averaged particle velocity of the individual particles (Figures 9A and 9B). The mean of the particle velocity in the area for 0.22 and 0.11 seconds of analysis approximate each other, despite the temporal and spatial variability in individual particle velocities. Later we apply double averaging as a method of sampling the dune stoss slope, to facilitate trend analyses of the sand particle motion over the dune.

The sampling method does not distinguish between modes of transport. Observations of the time lapse images allow for visual identification of transport modes. We observe rolling, sliding and saltation and we observe lift off of particles over longer distance than of saltating particles. The latter way of transport occurs from entrainment by ejection caused by impacts. The different ways of particle transport occur simultaneously within a sample area.

Instantaneous particle velocities over the stoss slope

Instantaneous particle velocities over the dune stoss slope obtained by manual tracing of 161 particles over five subsequent time steps are presented in Figure 10. The dune stoss slope is separated into two sections and the probability distributions of the velocities show distributions that are best fit by a gamma distribution. The instantaneous velocities measured at the upper section of the stoss slope show a wider peak compared to the measurements at the lower section of the stoss slope. Differences in the probability of instantaneous velocities are minor (Figure 10 and Figure 11). Instantaneous velocities at the lower section of the stoss slope are lower compared to the upper section of the stoss slope. For all the manually traced particles the mean is 0.089 m/s and the variance is 0.0032.

The measurements of instantaneous velocities over the dune stoss slope in Figure 12 show that most measurements of instantaneous velocity occur in the central region of the figure. The measurements at the lower section of the stoss slope (blue dots) tend to show an 'egg-shape' towards the higher cross-stream velocities. Whereas the point cloud from the measurements at the upper section of the stoss slope (red crosses) tends to be 'v-shaped' towards the higher streamwise velocities. Concluding, the instantaneous particle velocities over the dune stoss slope vary according to a gamma distribution. Small differences in the shape of the distribution exist for the lower and upper section of the dunes stoss slope.

Particle velocities over a dune slope: instantaneous velocity from manual tracing compared to spatially averaged velocity from cross-correlation analysis

Particle velocities over the dune stoss slope obtained by manual tracing and by cross-correlation on IoD are presented in Figure 13). Studying the direction and the velocity magnitude of the particles, and their frequency of occurrence, both methods show main particle movements ranging from 0.05 to 0.10 m/s. Cross-stream displacement is minor compared to the observed streamwise displacement. Particle velocities faster than 0.2 m/s are not observed frequently. Applying cross-correlation, erroneous vectors can occur, and are unavoidable with most data (Thielicke and Stamhuis, 2014). A vector validation procedure is applied, in which velocities faster than 0.4 m/s are considered as errors. As such, all measured velocities are lower than 0.4 m/s. The cumulative probability of the instantaneous particle velocities obtained from manual tracing shows that 50% of the particle velocities are within 0.04–0.10 m/s (Figure 14). About 30% of the velocities are faster than 0.10 m/s and 20% are

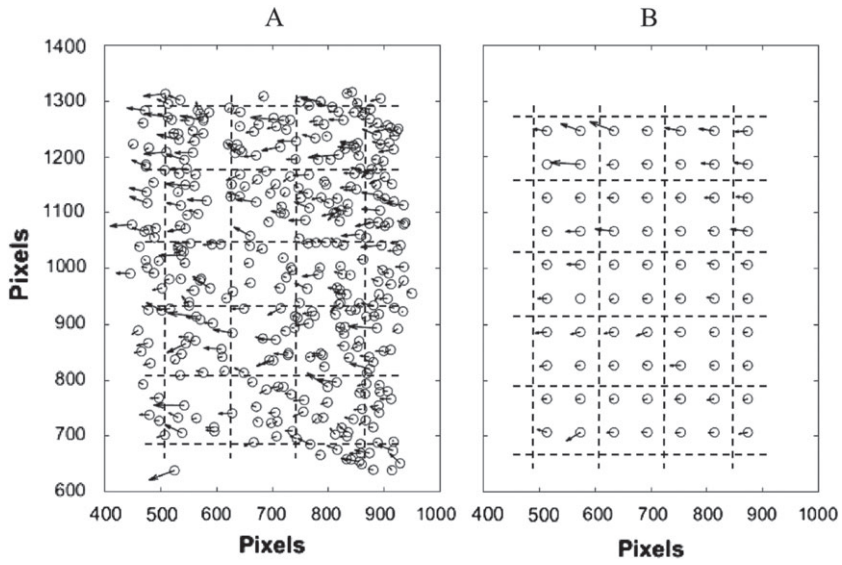

Figure 6. Comparison of velocity vectors obtained from manual tracing of particles (A), and cross-correlation on image of difference (IoD) with analysis area of 60 × 60 pixels, 0.013 × 0.13 m (B). Cross-stream width is 0.15 m and streamwise length is 0.12 m. Time step is 0.022 seconds. Agreement between the two methods increases for averaging four vectors into one and is represented with the grid.

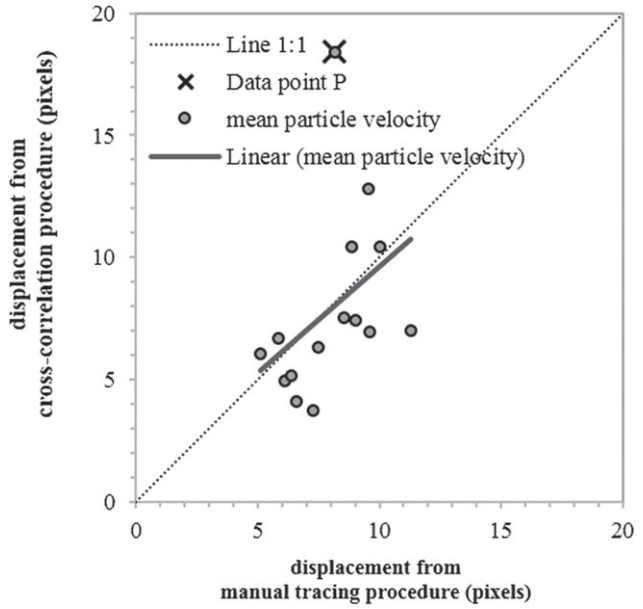

Figure 7. Comparison of mean particle velocity from manual particle tracing and cross-correlation on image of difference (IoD) for an analysis area of 0.026 by 0.026 m (see grid in Figure 6). Since there is a difference between the two methods in the number of moving particles that were identified to obtain mean particle velocity, a 1:1 agreement is not achieved. Data point 'P' shows a poor fit because the manual tracing is not suitable for events of high particle speed and high density of moving particles. Particles are observed to overtake each other, making particle identification impossible, with only a fraction of the moving particles traceable.

slower than 0.04 m/s. For the measurements based on cross-correlation analysis (PIV), which is a spatially averaged velocity, approximately 80% of the velocities are lower than 0.10 m/s, and 70% of the particle velocities are within 0.04–0.10 m/s. The measurements suggest that low particle velocity is less abundant. Though, time-averaging of the instantaneous velocities by manual tracing shows the same effect and gives that 70% of the particle velocities are within 0.04–0.10 m/s.

In Figure 15, the velocity distributions from the cross-correlation analysis of 950 velocities for an analysis time of 0.22 seconds, and of 4455 velocities for an analysis time of 1.11 seconds are shown. A comparison shows that the magnitude of the peak in the probability of the distribution (at ~0.1) and the associated particle velocity (~0.065 m/s) are similar, suggesting that the longer analysis time increases the likelihood of low (< 0.04 m/s) and high velocities (> 0.12 m/s), but does not modify the majority of the measurements and gives a closer overall fit to the gamma distribution. The mean of all streamwise velocities is 0.08 m/s and varies with ±0.005 m/s over time. The mean streamwise velocities are analysed over time and show that for a dune section the variation over time is ±0.01 m/s and for a cross-section the variation over time is ±0.02 m/s. Summarizing, comparison of distributions of the particle velocities for the different methods shows that time-averaged mean particle velocity from manual tracing compares to the velocities obtained from the spatially-averaged cross-correlation analysis. A longer analyses period does not affect the shape of the distribution, and increases the likelihood of occurrence of extremes (though extremes are rare).

Mean particle velocity over a dune slope

The mean particle velocities over the dune slope from cross-correlation analysis are presented in Figure 16–18. The measurements are taken at 32 cross-sections over the dune slope, with the cross-section being 0.026 by 0.156 m in size. Per cross-section, six velocities are obtained (double averaging procedure with t = 0.22 seconds). The velocities show a high variability and the variability was considered in the previous sections. Here, the focus is on the mean of the measurements and the mean value for every 1/10th section over the dune stoss slope is calculated. The results show that the mean streamwise particle velocity increases from the lower slope (0.06 m/s) to the dune crest (0.095 m/s). The regression slope changes ±10% for minor changes in the location of analysis area and spatial averaging procedure. The increase in particle velocity is strongest for the streamwise velocity (Figure 17), compared to the velocity magnitude (Figure 16). This is caused by slower streamwise velocities on the lower slope (~0.05 m/s). Additionally, the absolute value of the cross-stream velocity over the dune section shows strongest cross-stream movement on the lower part of the slope, whilst decreasing towards the middle part of the slope and increasing from the upper part of the slope to the

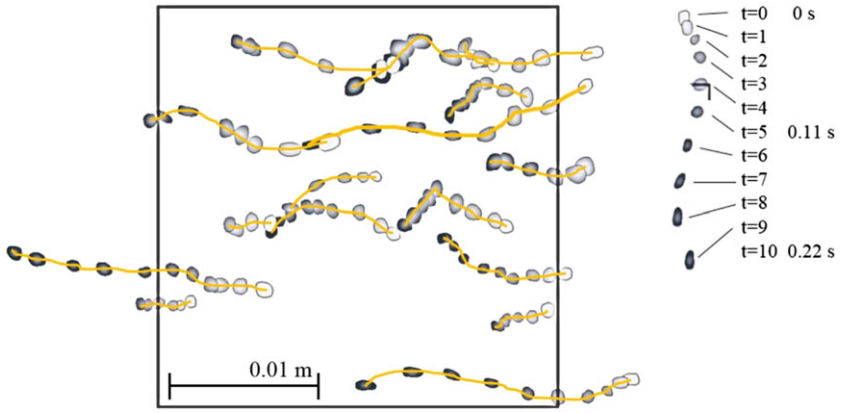

Figure 8. Particle displacement by manual tracing over 0.22 seconds and 10 frames (at time step 0.022 seconds). The colour intensity represents the time step. The box covers 120 by 120 pixels, which corresponds to an area of 0.026 by 0.026 m. The image illustrates variability in particle displacement between time steps and between particles. Particle displacement by manual tracing is obtained by drawing polygon features in ArcMap 10.5 for moving particles only. A polygon resembles the particle contour at a given time step. [Colour figure can be viewed at wileyonlinelibrary.com]

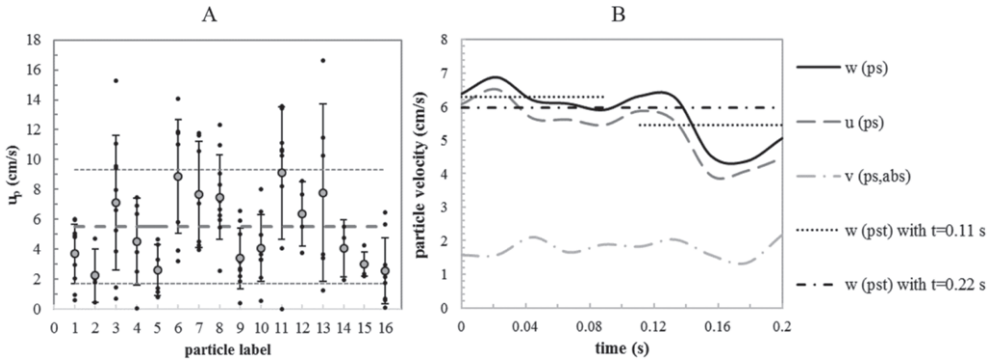

Figure 9. Streamwise instantaneous velocity in centimetres per second for 16 particles (black dots) and time-averaged streamwise velocity and standard deviation per particle (grey dots) over 6–10 time steps (A). The striped line is the spatial and time averaged velocity of the 16 particles and the grey dotted line represents the standard deviation (±1σ). The spatially averaged particle velocities are presented in (B). The abbreviations are mean streamwise particle velocity (*u*), mean cross-stream particle velocity (*v*), mean particle velocity (*w*), with (*p*) referring to particle velocity being spatially averaged (*s*) and/or time-averaged (*t*). Particles approached zero displacement in the time step before cessation and in case the displacement is in the cross-stream direction. Zero motion is excluded here because in an image of difference (IoD) a non-moving particle is filtered out.

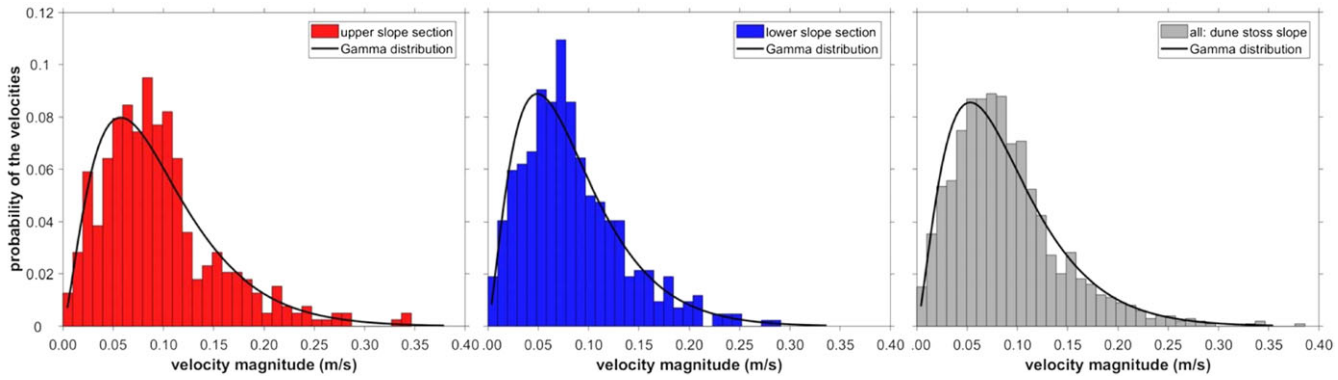

Figure 10. Velocity distributions obtained by manual tracing: instantaneous particle velocities over upper part of the slope, the lower part of the slope and over the dune stoss slope. The gamma distribution of all the measurements gives $a = 2.479$ (standard error 0.1048) and $b = 0.0359$ (standard error 0.00168). The mean is 0.089 and the variance is 0.003196. [Colour figure can be viewed at wileyonlinelibrary.com]

crest. By calculating the standard deviation divided by the mean, we show that the standard deviation is highest at the lower slope for the streamwise velocity and velocity magnitude and decreases towards the crest, although the variation between the dune sections is small. The standard deviation is about 30% of the mean value for streamwise velocity and magnitude of the velocity. Concluding, the mean of the particle velocities changes as a function of the dune slope. We identify three zones over the dune stoss slope: (1) region of fluctuating particle velocity, (2) region of increasing particle velocity, and (3) region of maximum particle velocity.

The number of particles that change position differ as a function of location on the dune slope. The number of active particles is largest close to the crest and lowest on the lower slope (Figure 19). Spatially, ~10% of the measurement area over the crest are covered with particles in motion. This size decreased to less than 1% close to the trough. Particle counts and identification of the area in motion are affected by noise in the IoD.

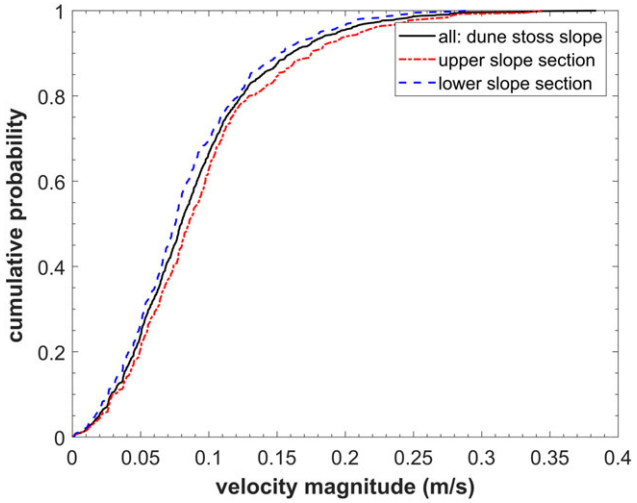

Figure 11. Cumulative frequency distribution of the instantaneous particle velocity over the dune stoss slope and separated for the lower and upper slope section. [Colour figure can be viewed at wileyonlinelibrary.com]

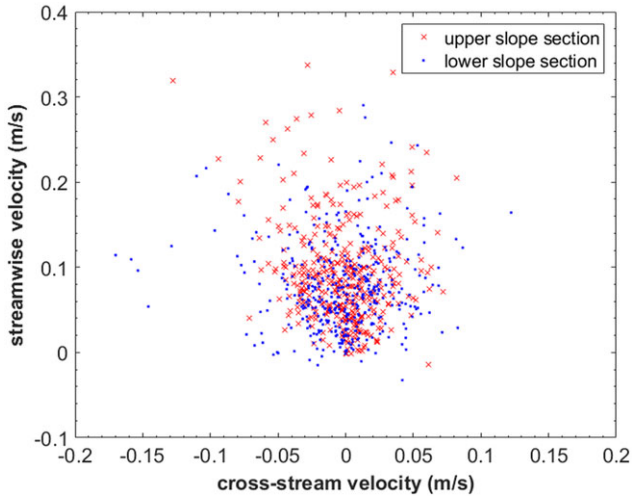

Figure 12. Instantaneous velocities over the dune stoss slope from manual tracing representing the measurements from the upper section of the dune stoss slope and the lower section of the dune stoss slope. [Colour figure can be viewed at wileyonlinelibrary.com]

Noise removal in the form of a pixel intensity threshold is applied. A stronger threshold would yield less activity. Accurate quantification for our measurements is challenging due to the small size of the particles and the large sampling area.

Discussion

Predictions of sediment transport using Shields parameter for rivers with dunes show acceptable performance on average. However, those predictors are limiting our understanding of local sediment transport over non-plain dune beds, for which gradients in sediment transport exist. Local bedload transport rate is the sum of the product of individual particle volume in motion and the streamwise velocity of the particle (Shim and Duan, 2017; Ballio *et al.*, 2018). No disruption of flow is the major advantage of using imagery to quantify sediment transport. Previously, imaging techniques have been used to record sediment transport of coarse particles, semi-fixed bed configurations, and a limited number of active particles in the sampling area. Dunes are composed of smaller sized sand particles, while the number of moving particles is high and the bed is mobile. We overcome the challenge in the present study and collected reliable measurements of particle velocity over the rising dune slope. Concluding, applying the PIV-based method of cross-correlation on IoD for studying mean particle velocity over a dune slope is well suited, and results allow the identification of spatial and temporal particle variability on the scale of centimetres.

Grain behaviour

Particle interactions, which are at the origin of onset and cessation of particle movement, and different modes of transport (rolling, sliding, saltation), cause variations in particle velocities of bedload. Our results identify the variability in particle velocity, and confirm generally observed behaviour of bedload at the particle scale: entrainment, displacement, distrainment and repose (Drake *et al.*, 1988). Previous studies document an exponentially decreasing probability of particle velocity for median grain size of 2.24 mm (Lajeunesse *et al.*, 2010) and 2.4 mm (Shim and Duan, 2017) and 0.5 mm (Roseberry *et al.*, 2012) whereas a gamma-like distribution was found for grains of 2 to 4 mm (Drake *et al.*, 1988) and 3 mm polybutylene terephthalate (PBT) grains (Campagnol *et al.*, 2013) and for 0.85 mm grains in this study. As such, there is a contradiction in the distribution of particle velocities being measured. The question arises whether the discrepancy results from differences in the methods and low particle velocities are under/over represented in some studies, and/or that the distribution of velocities depends on the forcing of the bed. Our results indicate that the shape of the distribution of velocities differs over the lower section of the dune slope compared to the higher section of the dune slope (Figure 11). We conclude that the forcing of the bed influences the probability of particle velocities. Time-averaging and spatial averaging of velocities decreases the probability of occurrence of low particle velocity for our measurements (Figure 14). The latter will be more strongly reflected in the mean of the particle velocity, than in the median of the particle velocity. A (simplified) theoretical framework on the essential parameters is needed to quantify sediment transport from the particle scale to the dune scale. Presently our understanding of the effect of bed forcing on sand transport is limited, with continued discussion on local shear stress quantification (Yager *et al.*, 2018). Visualization techniques are promising tools to further elaborate on the knowledge gap.

Particle motion over a dune slope and comparison to other studies

An automated PIV-based method is used to obtain mean particle velocities at different sections over a dune slope. The results show an increase of mean particle velocity from the lower slope towards the crest. Mean streamwise particle velocity at the crest is 0.09–0.10 m/s, while mean streamwise velocity at the lower slope is 0.04–0.065 m/s. Variability in particle velocity is high, represented by a high standard deviation compared to the mean and is characteristic for bedload motion. Whilst averaging over space and time leads to a consistent mean value of particle velocity that changes as a function of the dune slope. Commonly, the average dimensionless shear stress (Shields parameter) is used to compare experimental flow conditions. The results we present were obtained from experiments with Shields parameter and particle mobility similar to experiments by Lajeunesse *et al.* (2010) as seen in Figure 1. Their studies used low water depths (6–14 mm), eliminating dune formation.

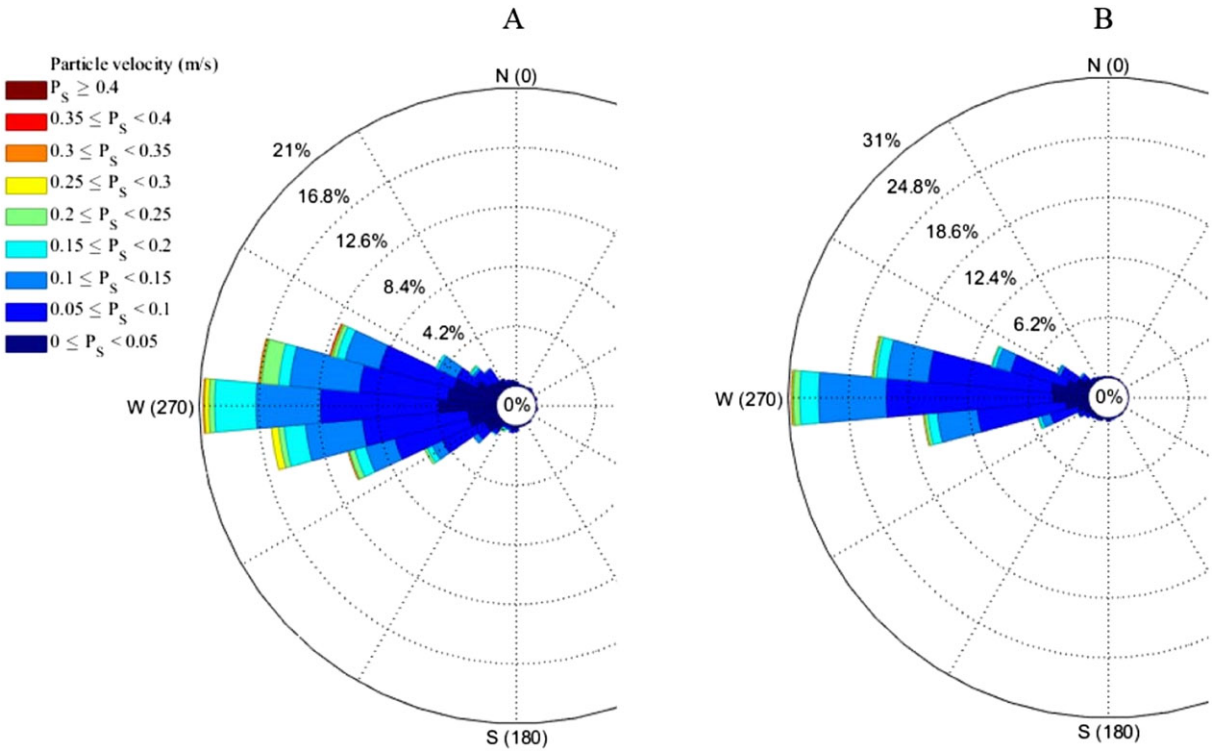

Figure 13. Rose plot presents particle velocity over a dune slope with W (270) the streamwise direction. Data consists of 990 particle velocities in 0.11 seconds of measurements from manual tracing (A) and 4455 velocities in 1.11 seconds of measurements from cross-correlation on image of difference (IoD) (B). [Colour figure can be viewed at wileyonlinelibrary.com]

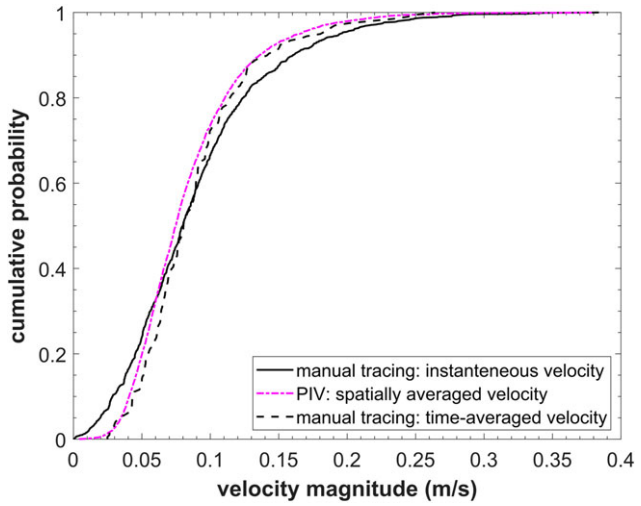

Figure 14. Cumulative frequency distribution of the instantaneous particle velocity over the dune stoss slope, the time-averaged instantaneous particle velocities and the spatially averaged velocity measurements from particle image velocimetry (PIV). [Colour figure can be viewed at wileyonlinelibrary.com]

Measurements of sediment transport by Lajeunesse *et al.* (2010) show that particle motion is dominated by the mean value of the bed shear stress. In dune fields, the dune geometry affects flow velocity and water depth. Local shear stresses increase over the dune slope (McLean and Smith, 1986). We identify three regions over the dune stoss slope (Figure 16). The region of increasing particle velocity and the region of maximum particle velocity resemble observed flow behaviour over dunes: increasing flow velocity over the dune resulting from flow conversion and compressing streamlines within the boundary layer over the rising stoss slope with maximum velocity at the crest, as shown by Best (2005). The increasing bed shear stress is, according to our measurements, represented with the increase in the mean value of particle velocity over the dune stoss slope. The particle activity increases from the lower slope towards the crest (Figure 19), which corresponds with the findings of Lajeunesse *et al.* (2010) despite the differences in the setting of the experiments. They show that above the threshold for motion, the number of moving particles per unit bed area increases linearly with the bed shear stress, minus critical bed shear stress. With our camera and illumination set-up, we were not able to accurately quantify the number of particles in motion and therefore we do not directly compare the findings. The question arises whether it is equally valid to conclude that grain velocities do not increase meaningfully over the dune stoss slope, and that the spatial and temporal variability in speed is far more dominant than an average trend. The latter would fit a potential model where grain velocity is not strongly dependent on the bed forcing, and that increases in overall bed-forcing, as that along the stoss slope, result in higher numbers of grains in motion instead. Our measurements show minor differences in mean particle velocity over the dune stoss slope, and minor differences in the shape of the frequency distribution suggesting that grain velocity is dependent on the bed forcing.

We observe that the variability in mean particle velocity is highest on the lower slope, and decreases towards the upper slope. It does not further decrease towards the crest. An explanation for highest variability on the lower section of the dune stoss slope is the occurrence of sweep-transport events. Visual observations indicate that sweep-transport events temporarily increase the number of moving particles and velocity of the moving particles (though the movement rapidly ceased). These events were observed more frequently on the lower section of the dune stoss slope. Also, the sweep-transport events increase the displacement in the cross-stream direction, explaining the higher absolute cross-stream velocity presented in Figure 18. Sediment transport is initiated at the lower slope and although we do not have measurements of the velocity fluctuations near the bed, we assume that the point where we observe continuous downstream directed sediment transport coincides with

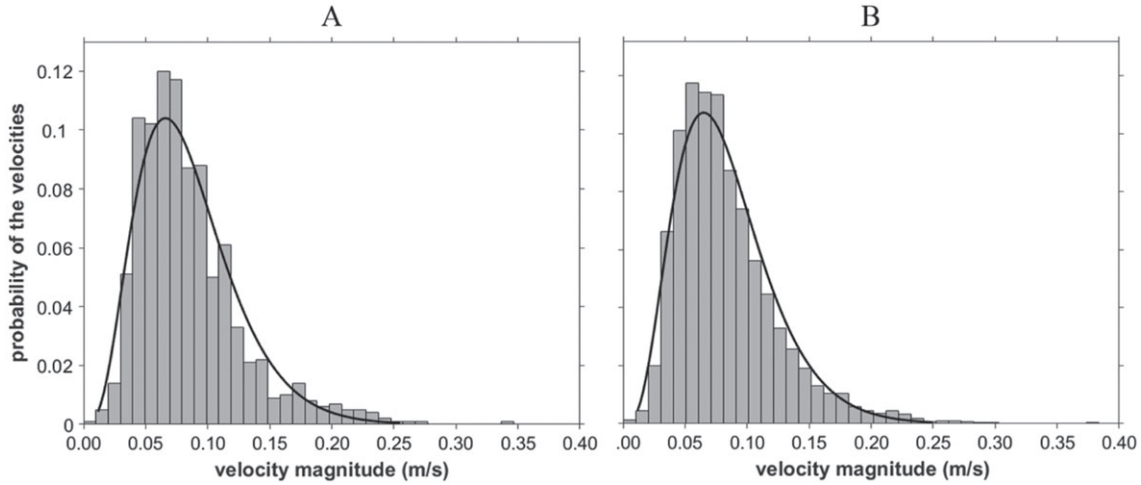

Figure 15. Velocity distribution of spatially averaged velocities obtained from the cross-correlation on image of difference (IoD): particle velocities over 0.22 seconds of measurements (A) and 4450 particle velocity magnitudes in 1.11 seconds of measurements (B).

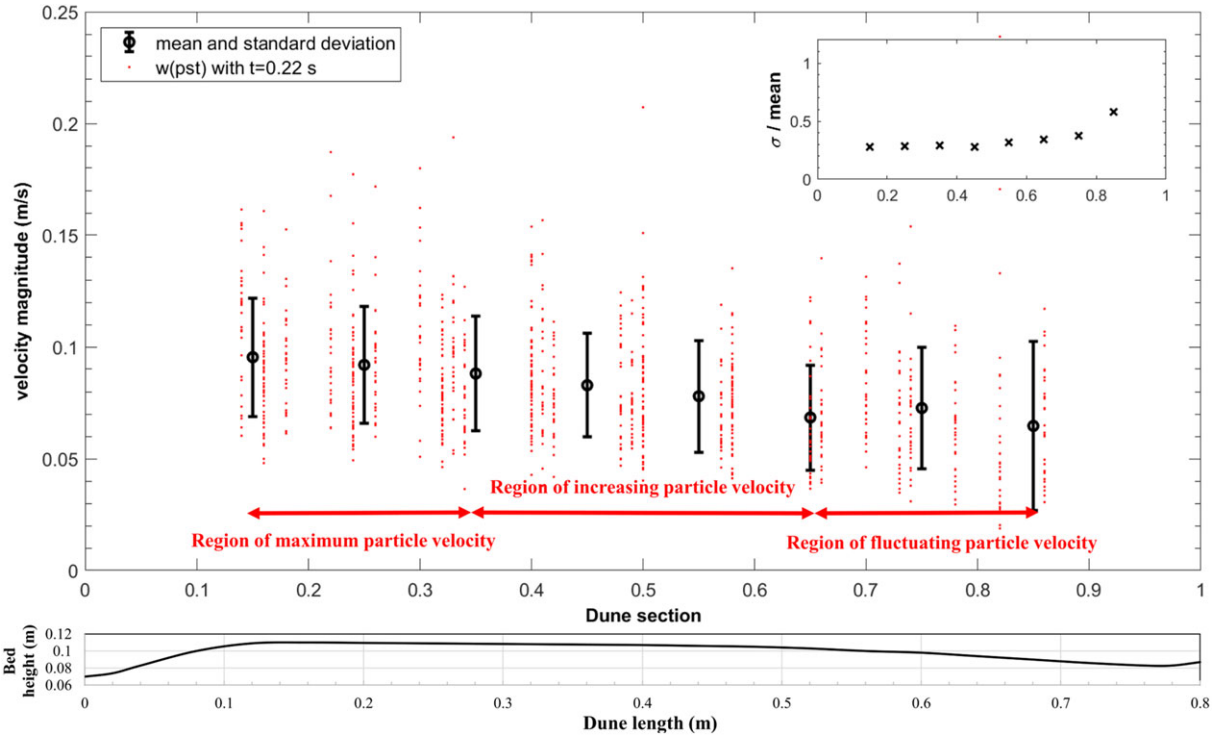

Figure 16. Velocity magnitude with standard deviation of particles according to cross-correlation on image of difference (IoD) over a dune slope for 1.11 seconds of measurements. [Colour figure can be viewed at wileyonlinelibrary.com]

the flow reattachment point. It is our observation that sweep-transport events are generated upstream and downstream of the (assumed) flow reattachment point. Some of the sweep-transport events pass by the flow reattachment point. Their contribution to the number of particles in motion and the direction of the particle motion on the lower slope is important. Sweep-transport events were few on the upper slope compared to the lower slope. Whereas, over the upper section of the dune slope superimposed bedforms were observed frequently. A superimposed bedform causes local increases and decreases in particle velocity (and activity) and in Terwisscha Van Scheltinga *et al.* (2018) we find maximum flux to coincide with the location of a superimposed bedform. Further work is needed to quantitatively relate the effect of sweep-transport events and superimposed bedforms to sediment transport over dune geometries.

Quantification of sediment mass flux over dunes using imagery and future work

Our image sequences show the top layer of the sediment. When assuming the sediment transport layer has a maximum thickness of particle size, it is theoretically possible to quantify the volume of sediment transport over dunes, using only plan view images. The sediment mixture consisted of particle sizes ranging from 0.65 mm to 1.15 mm (D_{16} and D_{90}), with a median particle size of 0.85 mm. This corresponds to three to five pixels covering a particle. The particles were often larger than five pixels, as particle velocity influenced the number of pixels covering a sediment particle. The higher the velocity, the larger the particle appeared in an image. We based displacement on the centre of the particle. Therefore, displacement was not influenced by particle size nor particle speed. The field of view of our

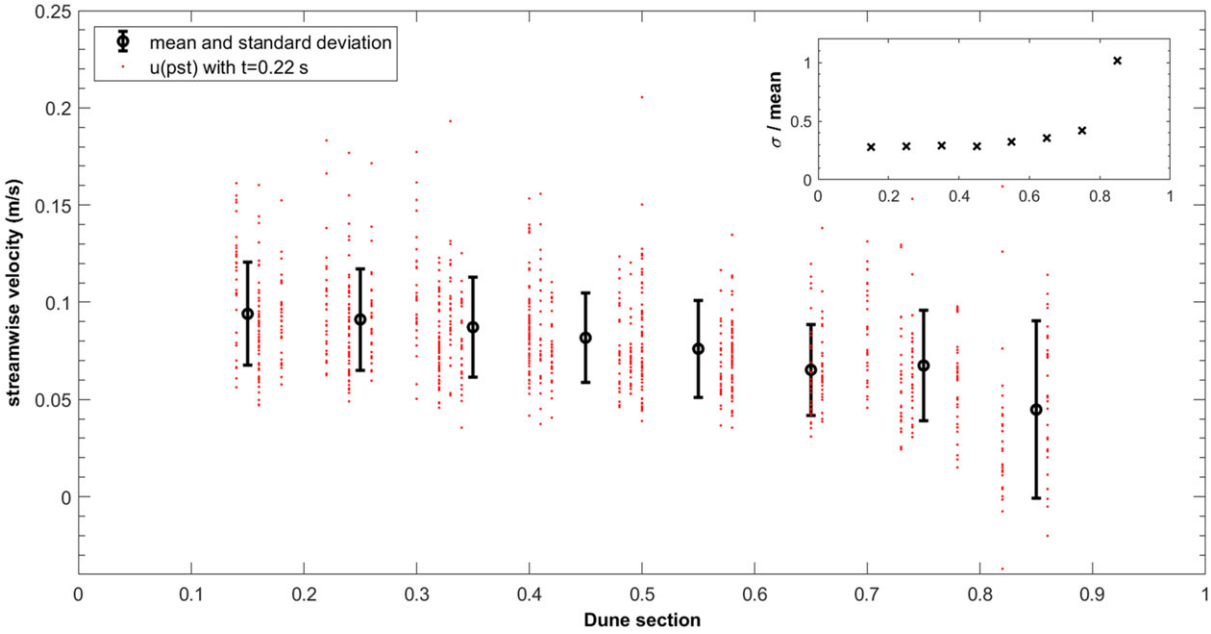

Figure 17. Mean streamwise velocity with standard deviation of particles according to cross-correlation on image of difference (IoD) over a dune slope for 1.11 seconds of measurements. [Colour figure can be viewed at wileyonlinelibrary.com]

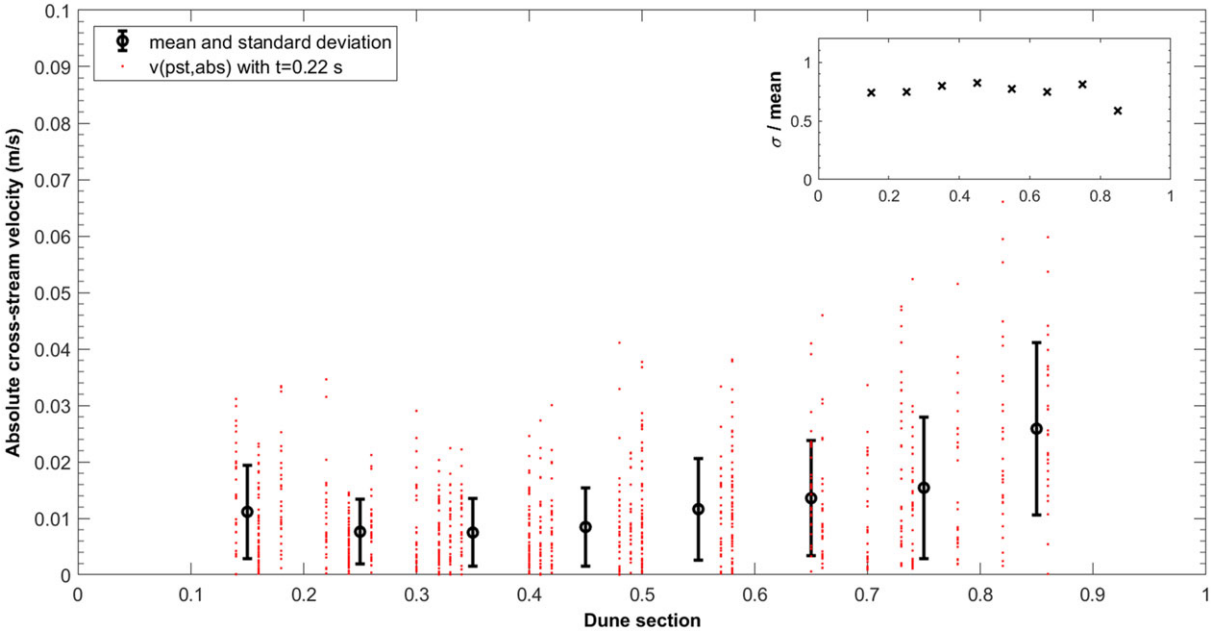

Figure 18. Absolute cross-stream velocity with standard deviation of particles according to cross-correlation on image of difference (IoD) over a dune slope for 1.11 seconds of measurements. [Colour figure can be viewed at wileyonlinelibrary.com]

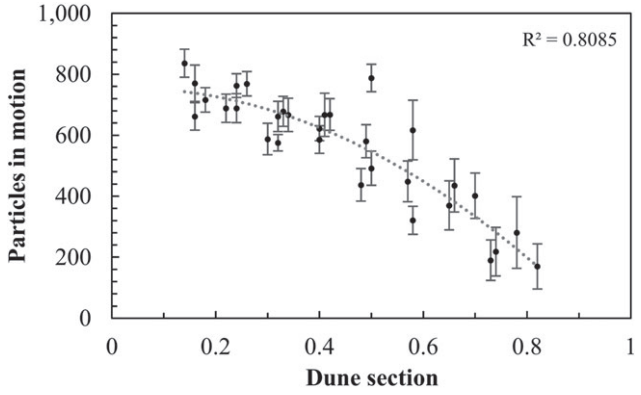

Figure 19. Particle motion over the dune stoss slope from image of difference (IoD) for 32 cross-sections over the dune stoss slope.

recordings and the corresponding exposure limited the analysis of different sand sizes. The light-coloured particles appear as a bright spot in the images and particle boundary is easily distinguished, while the displacement of the darker coloured particles was hardly detected. Thus, the displacement of the dark-coloured particles in the mixture was underrepresented. Concluding, we collected reliable measurements of streamwise velocity of the particles though quantification of the volume of moving sand over dunes using imagery is challenging. At this stage, practical limitations relevant for the study on dunes are: (a) consumer-grade camera's recording at high frame rate (> 90 frames per second) are generally limited in their resolution, (b) image quality decreases for increasing water depth, (c) water clarity reduces for increasing flow rates, (d) thickness of sediment transport layer has to be in the range of particle size for the plan view of the camera, (e) for quantification of mass flux

of a mixed sand over dunes (without the use of tracer particles) extensive post-processing on the imagery is required to account for the variability in sediment characteristics (size, shape, colour) and to account for the high variability in particle movement and for the interactions between particles while they move and (f) the sloped bed requires calibration to account for changing length scales and lens distortion due to water refraction.

Conclusions

This work presents measurements of particle velocities of the mobile bed over a dune. Experimental and numerical modelling studies indicate that the flow velocity over a dune is fluctuating, accelerating over the dune stoss slope and decelerating over the dune trough. A PIV-based cross-correlation technique on IoD was used to measure particle velocities over a rising dune slope. The mean streamwise particle velocity increases from the lower slope (0.06 m/s) to the dune crest (0.095 m/s). The measured increase in mean particle velocity agrees with the hypothesis that particle motion is dominated by the mean value of the bed shear stress. Over the dune slope, three regions are distinguished: (1) region of fluctuating particle velocity, (2) region of increasing particle velocity, and (3) region of maximum particle velocity. Our results imply that several processes cause deviations from the mean. Manual tracing of instantaneous velocities showed that the forcing of the bed influences the probability of particle velocities. The standard deviation of the mean particle velocity is affected by the slope location and decreases from the lower slope towards the upper slope. We provide a discussion in the context of general onset and cessation of sediment transport, the effect of the reattachment zone, sweep-transport events and of superimposed bedforms. Concluding, manual motion tracing was used to explore the validity of applying an automated PIV-based cross-correlation technique on IoDs of the mobile bed. The automated method is suited for quantification of particle motion at the scale of centimetres. The measurements fill the gap between individual particle motion studies and time-averaged sediment transport measurements. We show that the method can be fully automated for the challenging condition of mobile beds, sloping beds and for sand particles moving closely together, allowing analysis of local gradients in bedload transport.

Acknowledgements—The authors would like to acknowledge Prof. Dr M.G. Kleinhans and Dr A. Baas for reviews and discussions and Dr W. Li, Dr R. Wilson, G. Kirby and T. Patrick for technical support.

References

Ballio F, Pokrajac D, Radice A, Hosseini Sadabadi SA. 2018. Lagrangian and Eulerian description of bed load transport. *Journal of Geophysical Research: Earth Surface* **123**: 384–408. https://doi.org/10.1002/2016JF004087.

Ballio F, Radice A. 2007. Grain kinematics in weak linear transport. *Archives of Hydroengineering and Environmental Mechanics* **54**: 223–242.

Best J. 2005. The fluid dynamics of river dunes: a review and some future research directions. *Journal of Geophysical Research: Earth Surface* **110**: F04S02. https://doi.org/10.1029/2004JF000218.

Bouguet J. 2010. Camera Calibration Toolbox for Matlab - complete documentation, http://www.vision.caltech.edu/bouguetj/calib_doc/index.html (Last updated October 14th, 2015).

Campagnol J, Radice A, Nokes R, Bulankina V, Lescova A, Ballio F. 2013. Lagrangian analysis of bed-load sediment motion: database contribution. *Journal of Hydraulic Research* **51**: 589–596. https://doi.org/10.1080/00221686.2013.812152.

Coffin D. 2009. Executable for decoding raw digital photos: dcraw.exe. http://www.centrostudiprogressofotografico.it/en/dcraw/. Accessed on 4 July 2017.

Drake TG, Shreve RL, Dietrich WE, Whiting PJ, Leopold LB. 1988. Bedload transport of fine gravel observed by motion-picture photography. *Journal of Fluid Mechanics* **192**: 193–217. https://doi.org/10.1017/S0022112088001831.

Fathel SL, Furbish DJ, Schmeeckle MW. 2015. Experimental evidence of statistical ensemble behavior in bed load sediment transport. *Journal of Geophysical Research: Earth Surface* **120**: 2298–2317. https://doi.org/10.1002/2015JF003552.

Furbish DJ, Fathel SL, Schmeeckle MW, Jerolmack DJ, Schumer R. 2017. The elements and richness of particle diffusion during sediment transport at small timescales. *Earth Surface Processes and Landforms* **42**: 214–237. https://doi.org/10.1002/esp.4084.

Guala M, Singh A, Badheartbull N, Foufoula-Georgiou E. 2014. Spectral description of migrating bed forms and sediment transport. *Journal of Geophysical Research: Earth Surface* **119**: 123–137. https://doi.org/10.1002/2013JF002759.

Heays KG, Friedrich H, Melville BW, Nokes R. 2014. Quantifying the dynamic evolution of graded gravel beds using particle tracking velocimetry. *Journal of Hydraulic Engineering* **140**(7): 04014027.

Kleinhans MG, Leuven JRFW, Braat L, Baar A. 2017. Scour holes and ripples occur below the hydraulic smooth to rough transition of movable beds. *Sedimentology* **64**: 1381–1401. https://doi.org/10.1111/sed.12358.

Knack I, Shen HT. 2015. Sediment transport in ice-covered channels. *International Journal of Sediment Research* **30**: 63–67. https://doi.org/10.1016/S1001-6279(15)60006-3.

Lajeunesse E, Malverti L, Charru F. 2010. Bed load transport in turbulent flow at the grain scale: experiments and modeling. *Journal of Geophysical Research: Earth Surface*: **115**: F04001. https://doi.org/10.1029/2009JF001628.

Lau YL, Krishnappan BG. 1985. Sediment transport under ice cover. *Journal of Hydraulic Engineering* **111**: 934–950. https://doi.org/10.1061/(ASCE)0733-9429(1985)111:6(934).

Lewis QW, Rhoads BL. 2015. Resolving two-dimensional flow structure in rivers using large-scale particle image velocimetry: an example from a stream confluence. *Water Resources Research* **51**: 7977–7994. https://doi.org/10.1002/2015WR017783.

Lockwood K, Grover P, Ferreira Da Silva AM. 2018. Quantification of bed-load transport over dunes. In *Conference Proceedings River Flow 2018*.

Luijk G. 2007. DCRAW tutorial. http://www.guillermoluijk.com/tutorial/dcraw/index_en.htm Last updated: 7 Mar 2017. Accessed on 26 June 2017

Maddux T, Nelson J, McLean S. 2003. Turbulent flow over three-dimensional dunes: 1. Free surface and flow response. *Journal of Geophysical Research: Earth Surface* **108**(F1): 6009. https://doi.org/10.1029/2003JF000018.

McLean SR, Smith JD. 1986. A model for flow over two-dimensional bed forms. *Journal of Hydraulic Engineering* **112**: 300–317. https://doi.org/10.1061/(ASCE)0733-9429(1986)112:4(300).

Mosbrucker AR, Major JJ, Spicer KR, Pitlick J. 2017. Camera system considerations for geomorphic applications of SfM photogrammetry. *Earth Surface Processes and Landforms* **42**: 969–986. https://doi.org/10.1002/esp.4066.

Nabi M, De Vriend HJ, Mosselman E, Sloff CJ, Shimizu Y. 2012. Detailed simulation of morphodynamics: 1. Hydrodynamic model. *Water Resources Research* **48**: W12523. https://doi.org/10.1029/2012WR011911.

Nabi M, De Vriend HJ, Mosselman E, Sloff CJ, Shimizu Y. 2013. Detailed simulation of morphodynamics: 2. Sediment pickup, transport, and deposition. *Water Resources Research* **49**: 4775–4791. https://doi.org/10.1002/wrcr.20303.

Nino Y, Garcia M. 1998. Experiments on saltation of sand in water. *Journal of Hydraulic Engineering* **124**: 1014–1025. https://doi.org/10.1061/(ASCE)0733-9429(1998)124:10(1014).

Radice A, Malavasi S, Ballio F. 2006. Solid transport measurements through image processing. *Experiments in Fluids* **41**: 721–734. https://doi.org/10.1007/s00348-006-0195-9.

Raffel M, Willert CE, Wereley S, Kompenhans J. 2007. *Particle Image Velocimetry: A Practical Guide*. Springer: Berlin; 79–96; 123–176.

Roseberry JC, Schmeeckle MW, Furbish DJ. 2012. A probabilistic description of the bed load sediment flux: 2. Particle activity and motions. *Journal of Geophysical Research: Earth Surface* **117**: F03032. https://doi.org/10.1029/2012JF002353.

Shim J, Duan JG. 2017. Experimental study of bed-load transport using particle motion tracking. *International Journal of Sediment Research* **32**: 73–81. https://doi.org/10.1016/j.ijsrc.2016.10.002.

Singh A, Foufoula-Georgiou E. 2013. Effect of migrating bed topography on flow turbulence: implications for modelling sediment transport. In *Coherent Flow Structure at Earth's Surface*, Venditti JG, Best JL, Church M, Hardy RJ (eds). John Wiley & Sons: Chichester; 323–339.

Southard JB, Boguchwal LA. 1990. Bed configurations in steady unidirectional water flows. Part 2. Synthesis of flume data. *Journal of Sedimentary Petrology* **60**: 658–679.

Sumner R. 2014. Processing RAW images in MATLAB. In *Instructional Document*. https://rcsumner.net/raw_guide/RAWguide.pdf

Tal M, Frey P, Kim W, Lajeunesse E, Limare A, Métivier F. 2012. The use of imagery in laboratory experiments. *Fluvial Remote Sensing for Science and Management*. John Wiley & Sons: Chichester; 299–321.

Terwisscha Van Scheltinga RC, Friedrich H, Coco G. 2018. A PIV-based method to measure spatial gradients in bedload transport over a dune. In *Conference Proceedings River Flow 2018*.

Thielicke W, Stamhuis EJ. 2014. PIVlab – towards user-friendly, affordable and accurate digital particle image velocimetry in MATLAB. *Journal of Open Research Software* **2**: 10.

Tsubaki R, Baranya S, Muste M, Toda Y. 2018. Spatio-temporal patterns of sediment particle movement on 2D and 3D bedforms. *Experiments in Fluids* **59**: 93. https://doi.org/10.1007/s00348-018-2551-y.

Van Rijn LC. 1984. Sediment transport, part III: bed forms and alluvial roughness. *Journal of Hydraulic Engineering* **110**: 1733–1754. https://doi.org/10.1061/(ASCE)0733-9429(1984)110:12(1733).

Van Rijn LC. 1987. Sediment transport, part I: bed load transport. *Journal of Hydraulic Engineering* **113**: 1189–1190. https://doi.org/10.1061/(ASCE)0733-9429(1987)113:9(1189).

Venditti JG. 2007. Turbulent flow and drag over fixed two- and three-dimensional dunes. *Journal of Geophysical Research: Earth Surface*: 112. https://doi.org/10.1029/2006JF000650.

Venditti JG, Lin CYM, Kazemi M. 2016. Variability in bedform morphology and kinematics with transport stage. *Sedimentology* **63**: 1017–1040. https://doi.org/10.1111/sed.12247.

Vollmer S, Kleinhans MG. 2007. Predicting incipient motion, including the effect of turbulent pressure fluctuations in the bed. *Water Resources Research* **43**: W05410. https://doi.org/10.1029/2006WR004919.

Westerweel J, Geelhoed PF, Lindken R. 2004. Single-pixel resolution ensemble correlation for micro-PIV applications. *Experiments in Fluids* **37**: 375–384. https://doi.org/10.1007/s00348-004-0826-y.

Yager EM, Schmeeckle MW. 2013. The influence of vegetation on turbulence and bed load transport. *Journal of Geophysical Research: Earth Surface* **118**: 1585–1601. https://doi.org/10.1002/jgrf.20085.

Yager EM, Venditti JG, Smith HJ, Schmeeckle MW. 2018. The trouble with shear stress. *Geomorphology* **323**: 41–50. https://doi.org/10.1016/j.geomorph.2018.09.008.